Engine Bearing Design

11

Within any given engine a large number of bearings incorporating several design, material, and operational variations are seen. While needle, ball, or roller bearings are sometimes seen in automotive and heavy-duty engines the majority of engines for these applications use primarily plain bearings. Roller bearings are receiving increasing attention due to their lower oil supply requirements and potential for reduced friction and parasitic losses in automotive engines. Increased space requirements, and in the case of connecting rod bearings increased rotating mass, must be weighed against potential attractions. Automotive engine examples of ball and roller bearing are seen in valvetrain and balancer shaft bearings. The discussion presented in the following sections will be limited only to plain bearings.

11.1 Hydrodynamic Bearing Operation

Crankshaft rod and main bearings, camshaft bearings and (if used) roller follower bearings operate under fully hydrodynamic lubrication under all conditions except engine start-up. Bearing areas at each of these locations are determined such that hydrodynamic operation is ensured under maximum load conditions. The camshaft and roller follower bearings are continuous shell, single-piece bearings. In most multi-cylinder engines assembly requires the use of split bearing shells at the crankshaft main and connecting rod bearings.

The bushings found at the piston pin, rocker levers, and (if used) cam followers experience stop-and-start motion even when the engine is operating at a steady speed. The stop-and-start motion precludes hydrodynamic operation, so these bearing surfaces are designed to operate under mixed film lubrication. Bearing area and material selection decisions are based on controlling the wear rates within limits defined by expected engine life.

K. Hoag, B. Dondlinger, *Vehicular Engine Design,* Powertrain,
DOI 10.1007/978-3-7091-1859-7_11

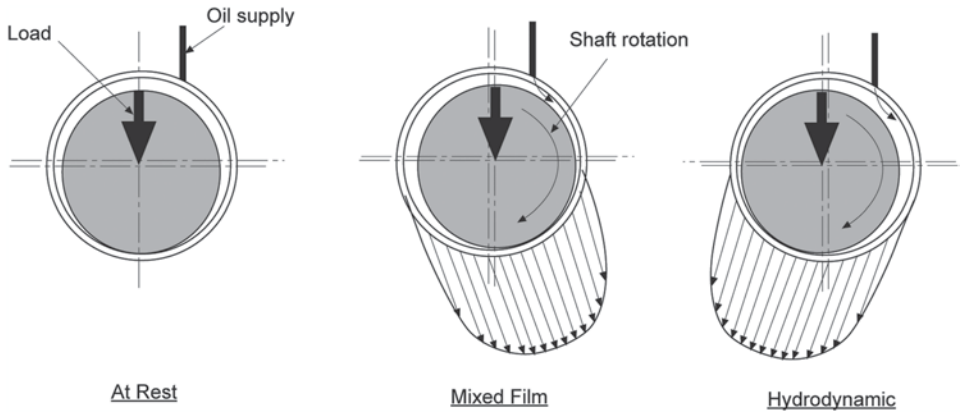

Fig. 11.1 Plain bearing operation, showing start-up and fully hydrodynamic conditions

Hydrodynamic bearing operation is summarized in Fig. 11.1. In each of the cases shown in the figure the shaft is loaded in the vertical direction. The bearing clearance is exaggerated to aid in viewing the operating characteristics. In the panel at the left the shaft is at rest and thus its contact with the bearing is centered about the vertical. The shaft is offset from the bearing centerline by the radial clearance between the shaft and journal (bearing surface).

In the center panel of the figure the shaft begins rotating. Pressurized oil is now being fed to the bearing as shown, and the spinning shaft carries oil into the gap between the shaft and bearing. While the oil film "lifts" the shaft away from the bearing the clearance (oil film thickness) is not yet sufficient to completely separate the surfaces. Because of the metal-to-metal contact between the shaft and bearing the shaft tends to "walk up" the bearing, and the ***contact patch*** is centered upstream from the direction in which the load is applied. The contact patch is the region between the shaft and the bearing over which load is distributed. The minimum oil film thickness occurs at some location within the contact patch. During this time of mixed film lubrication the shaft offset within the journal is the difference between the radial clearance and the minimum oil film thickness, and the direction of the offset is upstream of the direction from which the load acts.

As shaft speed increases and additional oil is supplied the film thickness increases sufficiently to completely separate the shaft from the bearing. The film thickness required for complete separation is dependent on the shaft and bearing surface finishes. The transition to fully hydrodynamic operation is shown in the panel on the right side of Fig. 11.1. Once hydrodynamic operation is achieved the contact patch shifts downstream of the applied load direction as shown. The shape and location of the oil film pressure distribution can be theoretically derived from fluid mechanics for ideal hydrodynamic operation.

From this discussion the variables impacting hydrodynamic operation can be identified. The combination of the magnitude of applied load and the bearing diameter and width define the resulting oil film pressure. The oil viscosity, the radial clearance between

the shaft and journal, and the shaft speed work to define both the leakage rate and the film thickness with given oil film pressure; the oil supply rate must be maintained at or above the leakage rate. Finally, the shaft surface finish determines the minimum oil film thickness required for hydrodynamic operation.

It should be noted that this description of hydrodynamic bearing operation assumes zero deflection of either the shaft or the journal. Engines often experience significant journal deformation, resulting in what is termed ***elasto-hydrodynamic*** operation. The elasticity of the journal may be sufficient to result in two or three distinct minimums in the oil film thickness, and two or three distinct film pressure peaks. Block movement and shaft deflection may further impact the instantaneous relationship between the shaft and journal centerlines. Machining tolerances impact the initial alignment between shaft and journal and must also be controlled. Each of these effects will be further discussed later in this chapter.

As shown in the middle and right panels in Fig. 11.1 the load distribution causes a distribution of film pressures. The film pressures are well above the supplied oil pressure; this is an important point, necessitating that whenever possible the oil supply drilling be placed upstream of the contact patch and not within it for two reasons. First, because pressures within the contact patch are above the supply pressure oil flow from a drilling directly into the contact patch would be effectively shut off when the bearing was loaded. Second, the diameter of the oil drilling would be lost from the bearing contact area.

Before leaving the general discussion of hydrodynamic bearing operation the various operating limits for plain bearings must be considered. The general limits are identified in Fig. 11.2 as a function of shaft speed and bearing load. The axes in this figure are shown without numbers since the specific limits are strongly dependent on the engine and the lubricant properties. As has already been discussed as load is increased the bearing is limited by asperity contact. Since this is the limit determined by the transition to and from hydrodynamic operation it should not be surprising that higher loads can be accommodated

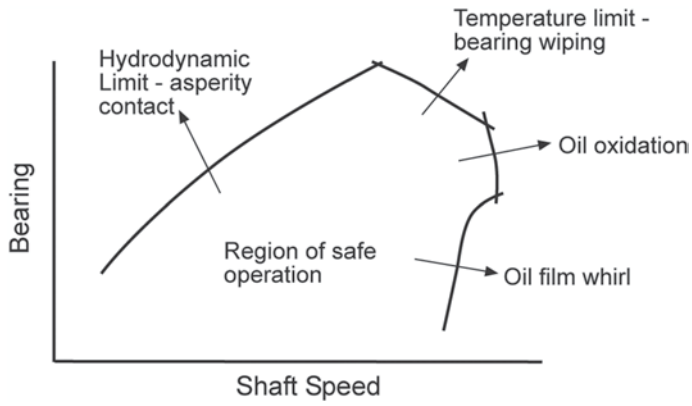

Fig. 11.2 Limiting regimes for plain bearing operation

as the shaft speed is increased. At high shaft speeds the shear forces within the lubricant result in significant temperature increases. The speed and load are limited by temperature limits of the bearing itself—the bearing surface may reach the temperature at which the material locally melts and streaks or wipes along the shaft. At slightly lower loads the temperature may not be sufficient to melt the bearing surface, but a longer term phenomenon is lubricant oxidation breakdown due to the elevated temperature. Finally, at high shaft speeds and light loads shear within the oil film may result in turbulent vortices causing the oil to spin or whirl within the film. This increases friction, oil foaming and cavitation, and may then result in damage to the bearing surface.

11.2 Split Bearing Design and Lubrication

As was stated at the outset of this chapter the need to assemble the bearing journal around a shaft necessitates the use of split bearings for the crankshaft main and rod bearings in multi-cylinder engines. The basic features of split bearing design are summarized in Fig. 11.3. The journal and the bearing shell are split along the shaft centerline as shown. If the joint shown represents a main bearing, the bearing cap is bolted to the block after installation of the crankshaft; if the joint shown is a connecting rod the rod is clamped around the shaft, and is held in place with the rod bearing cap. In either case the bearing shell is clamped in position as the cap is installed. The two halves of the bearing shell are each made slightly larger than their respective halves of the journal, resulting in a bearing ***crush load*** when the cap is clamped in place. The crush load is intended to create a uniform outward force around the perimeter of the bearing shell, holding it firmly in place. This is a critical design variable, as too little crush results in bearing shell movement against its journal, and fretting wear on the back surface of the shell. With time the

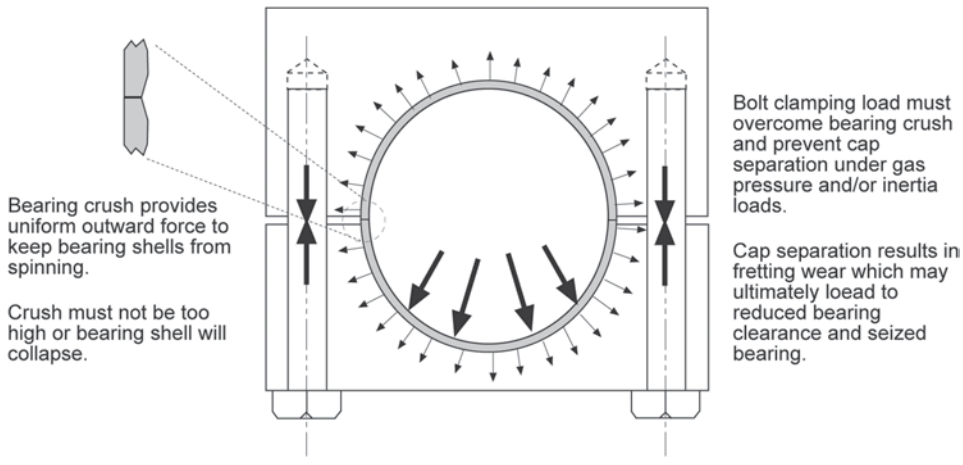

Fig. 11.3 Split bearing shell design principles

bearing loses load carrying capability due to loss of supporting material, and this may in turn lead to a bearing fatigue failure due to overload of the remaining material. If the crush load is too great it may damage the bearing shell during assembly, and may force bearing material against the shaft. High crush load also contributes to cap separation. Firing forces on the main bearings and inertia forces on the rod bearings both act in the direction of the cap, tending to pull the cap away from its seat. If these forces (along with the reaction to bearing crush) are high enough to momentarily separate the cap from its mating surface fretting wear results at this joint. Over time the resulting material loss reduces the bearing clearance, and may ultimately lead to bearing scuffing or seizure.

The peak loads resulting from firing forces act on the cap portion of the main bearing. Main bearing bolt design options for preventing cap separation and minimizing unwanted journal movement were discussed in Chap. 8. A further main bearing design challenge is that of supplying lubricant where it is most needed. As was discussed in the first section of this chapter ideal placement of the oil supply drilling is immediately upstream of the contact patch. In the case of the main bearing this would require placing the oil drilling in the main bearing cap, adding considerably to cost even if space were available. The practical requirement is to supply the main bearings with oil from cross-drillings from the oil rifle. The cross-drillings supply oil into the block portion of the main bearing journal, from where it must traverse along the bearing surface to where it is most needed. A design guideline is thus to place the location of the cross-drilling as close as is practical to the cap mating surface on the side of the engine that will result in crankshaft rotation carrying the oil directly toward the cap. Since this design guideline impacts placement not only of the cross-drillings but the oil rifle drilling, the oil pump, and the camshaft (any component or system requiring pressurized oil) it may not be possible to achieve in every engine design. Another design option is to place a groove in the center of the main bearing shell, carrying oil from the supply drilling around the entire bearing perimeter. This holds the advantages of supplying oil directly to the needed regions of the bearing, and better supplying the crankshaft drilling to the connecting rod bearings, but it also has the disadvantage of reducing bearing area by the width of the oil groove. Since bearing area is most needed (loads are highest) at the mid-position of the bearing cap another option is to place the oil groove only in the upper bearing shell, with a smooth transition eliminating the groove as the mid-position in the cap is approached. This option is very attractive from a design standpoint, but is chosen with caution because of the risk of reversing the bearing shells in the field.

The need for a thrust bearing surface at one of the crankshaft main bearings was previously discussed in Chap. 8. In most automotive engines the thrust surfaces are incorporated in one of the main bearing shells. In larger engines separate thrust bearings will be mounted adjacent to the main bearing shells on one bulkhead.

As with the main bearings, the direction and magnitude of loading seen by the rod bearings changes continually throughout the engine operating cycle. This is depicted in Fig. 11.4. The peak firing loads are seen just after TDC in the expansion stroke, and act near the center of the rod. A second peak results from the reciprocating inertia forces and

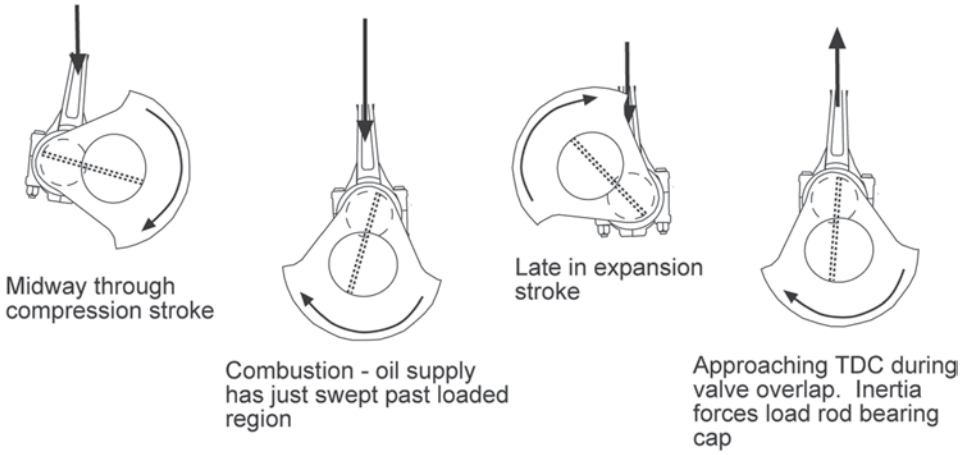

Fig. 11.4 Rod bearing loading at various points in the four-stroke operating cycle

is seen near TDC during the valve overlap period. It acts near the center of the rod cap. These forces will be further discussed in the next section.

The connecting rod bearing faces the unique situation of receiving its lubrication from a drilling in the spinning crankshaft. Pressurized lubricant is supplied to the main bearings, and from there passes through angled drillings in the crankshaft to reach the connecting rod bearings. This holds the advantage of sweeping oil around the entire bearing perimeter as the crankshaft spins. Unfortunately it also requires that the oil drilling break out in or very near the loaded region associated with the peak firing forces. The design objective is to angle the drilling such that it breaks out ahead of the TDC position. The oil drilling should sweep across the central region of the rod bearing, supplying a film of oil immediately before the peak loads are seen. The placement of the drilling is optimized within crankshaft geometry constraints.

11.3 Bearing Loads

The magnitude and direction of the forces acting on each connecting rod bearing can be calculated as a function of crank angle using the equations presented in Chap. 6. The forces include the resultant of the cylinder pressure and reciprocating forces transmitted through the connecting rod, and the rotational force contributed by the mass of the lower end of the connecting rod. Each of these forces and their calculation is identified in Fig. 11.5. The resulting bearing load is often depicted using polar load diagrams, two examples of which are given in Fig. 11.6. The trace shown in either figure is that of the tip of a vector whose origin is at the rod bearing centerline. At any crank angle position the length of the vector is proportional to the magnitude of the force applied to the bearing, and the direction indicates the direction in which the force acts. Using the polar load diagram one can clearly see the peak bearing force resulting from combustion and nearly

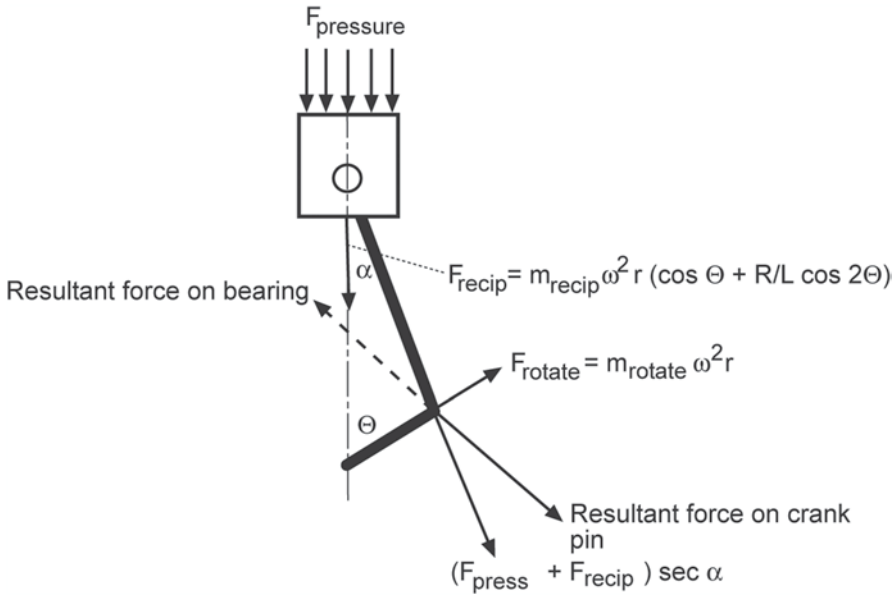

Fig. 11.5 Mechanisms leading to the resultant load seen by connecting rod bearings

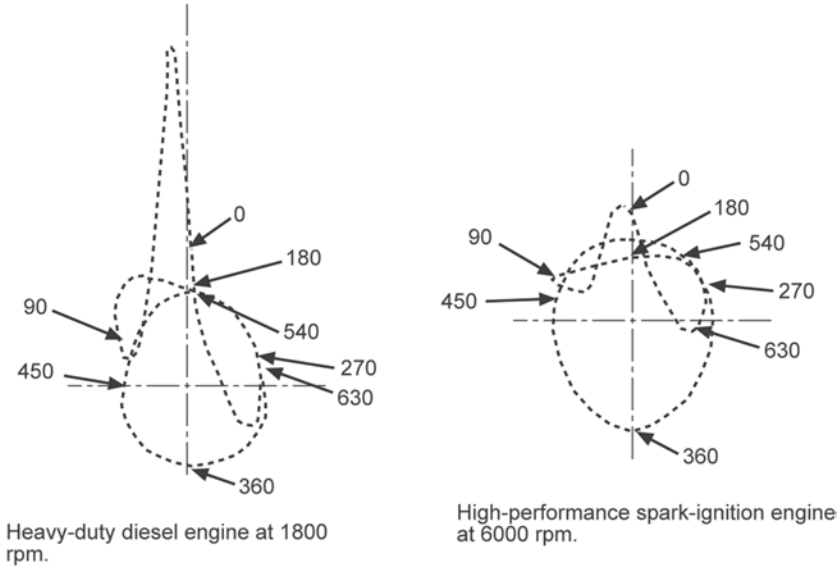

Fig. 11.6 Example polar load diagrams for rod bearings in two engine applications

centered along the rod axis (just after 0° crank angle in the figures, where zero has been chosen as TDC between compression and expansion). One crankshaft revolution later (360° crank angle) the piston is again at TDC during valve overlap. The cylinder pressure

is low and the inertia force resulting from deceleration of the piston assembly results in a load peak centered in the connecting rod cap. The relative magnitudes of firing pressure and inertia forces are quite different when comparing the two polar load diagrams in Fig. 11.6. The diagram shown on the left in Fig. 11.6 is that for a heavy-duty diesel engine, where cylinder pressures are quite high, and because the engine speed is relatively low, the inertia force is considerably lower. The case shown on the right in Fig. 11.6 is that of a high-performance spark-ignition engine. The engine speed is quite high, and the cylinder pressure is well below half that in the diesel engine. Several items of information important to the engineer can be gained from these polar load diagrams. The first is of course the peak load magnitude as this will be required in order to size the bearing and ensure that fully hydrodynamic operation is achieved. Second, the peak inertia load will be important in developing the connecting rod cap and the joint between the cap and rod. Finally, while the loads are much lower along the parting plane between the rod and cap they are not zero and very little bearing load can be handled along this plane. This becomes especially important in engines where the parting plane is placed on an angle. The polar load diagram provides guidance in ensuring that the parting plane is selected at a location where loading is as low as possible.

Figure 11.7 progressively identifies the loads seen by the main bearings. At least in theory the same calculation methods can be carried over to the main bearings, however the situation quickly becomes much more complex. The loads generated at each connect-

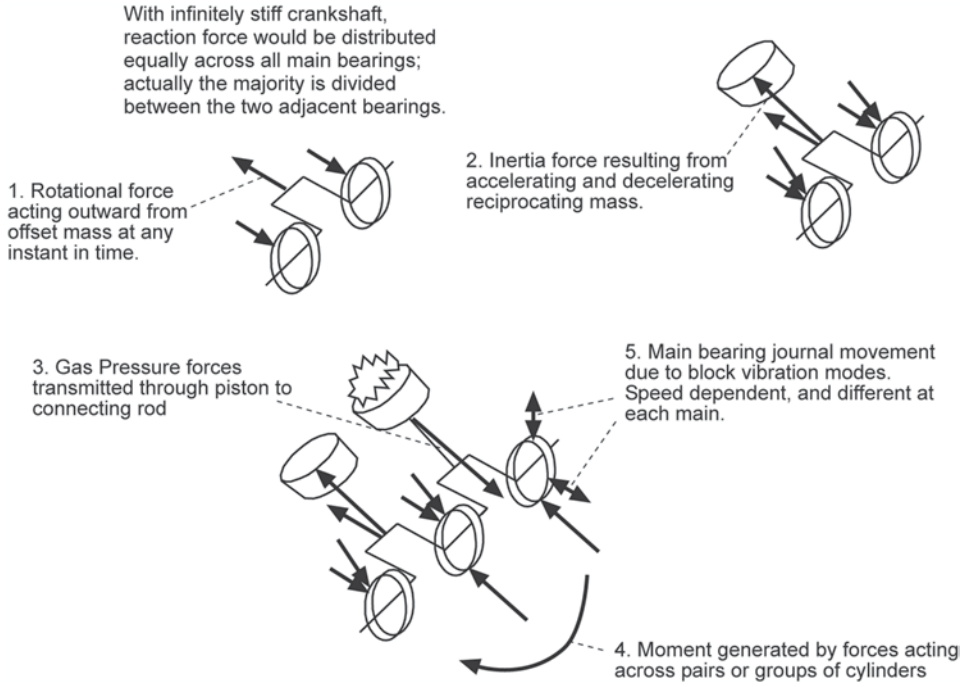

Fig. 11.7 Mechanisms leading to the resultant loads seen by main bearings

ing rod journal are the same as those seen at the rod bearings with the exception that the rotating mass now includes that of the crankshaft as well as the bottom end of the rod. If the crankshaft and cylinder block were infinitely stiff the load generated at each cylinder would be evenly distributed across all of the main bearings. In reality the majority of the load is divided between the two adjacent main bearings, with the remaining bearings seeing progressively smaller loads. In Chap. 6 moments resulting from dynamic couples between cylinders or groups of cylinders were identified. These too can be calculated, and their effects minimized or eliminated through crankshaft counterweight design as was discussed in Chap. 6. Up to this point the calculation of main bearing loads remains quite straight-forward though a bit challenging if the effect of crankshaft stiffness on load distribution across the main bearings is to be included. Unfortunately the situation is far more complicated. As a result of the block dynamics discussed in Chap. 10 the main bearing bulkheads shift with block mode shape—a function of block stiffness and engine speed. While these shifts are small they are often sufficient to significantly further load or unload a given main bearing.

Two examples of main bearing polar load diagrams are presented in Fig. 11.8. Because of the effect of block bending and twisting modes the polar load diagrams can vary significantly not only from one main bearing to another within a given engine, but at any given bearing as the engine speed changes. The diagram shown on the left in Fig. 11.8 is that for a vee engine, and at least two firing and two inertia peaks can be identified, but each is further skewed by block motion, and loads generated at throws further away on the crankshaft. The diagram on the right in Fig. 11.8 shows the simpler diagram of an in-line engine, but significant movement of the main bearing centerline has shifted the majority of the loading to one bearing quadrant. It should be clear from these examples that accurate characterization of the main bearing loads requires a coupled analysis that includes the effects of block motion and crankshaft bending.

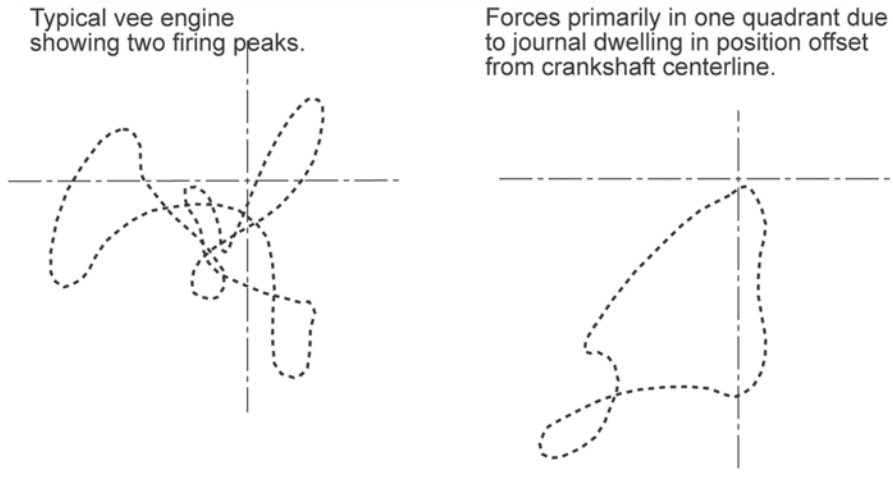

Fig. 11.8 Example main bearing polar load diagrams

While further examples are not shown here, similar bearing loading calculations can be made for the cam bearings, rocker levers, piston pins, and each of the other bearing locations within the engine. The cam bearings are designed for fully hydrodynamic lubrication. Many of the other bearing surfaces are subjected to continual start-and-stop motion, and thus metal-to-metal contact. Bearing design for both scenarios will be further discussed in the sections to follow.

11.4 Classical Bearing Sizing

Whenever possible, the foremost goal in developing a bearing is to ensure fully hydrodynamic operation under all conditions. This means that the oil film thickness throughout the loaded region must be sufficient to completely separate the "peaks" in the machined surface of the shaft from those on the bearing surface. The variety of parameters that must be considered in ensuring hydrodynamic operation were introduced in the opening section of this chapter. Most of these parameters will be further discussed as the classical computations of bearing film pressure and thickness are presented in this section, and advanced techniques designed to address deviations from the theoretical ideal are covered in the next section.

If one can assume that sufficient oil is present, that the bearing is under steady load, and that neither the shaft nor the journal experience any deflection a nearly exact solution for oil film thickness and pressure distribution can be derived from Reynolds' equation. The derivation was initially done for infinitely long bearings (no edge leakage, and uniform pressure across the bearing length), and was extended by Ocvirk (see the Recommendations for Further Reading) to include "short" bearings. The derivation is not repeated here, but the equation for film pressure as a function of position along the bearing width and around the perimeter is as follows. Pressure distributions as shown in Fig. 11.1 result.

$$P = \frac{3\mu U}{r c_r^2}\left(\frac{w^2}{4} - z^2\right)\frac{\left(\frac{e}{c_r}\right)\sin\theta}{\left(1+\left(\frac{e}{c_r}\right)\cos\theta\right)^3} \tag{11.1}$$

where:

P = film pressure
μ = absolute viscosity of the oil
U = surface velocity
R = bearing radius
c_r = radial clearance
w = bearing width

z = positive or negative distance from the center of the bearing
e = eccentricity of shaft centerline relative to journal centerline
θ = angular position from the location of maximum film thickness

A graphical presentation, shown in Fig. 11.9, and based on the dimensionless Sommerfeld number was developed by Ocvirk. The following example demonstrates its use in bearing sizing.

Example
A peak load of 222,400 N is applied to a bearing of 100 mm diameter and 50 mm width. The radial clearance is 0.05 mm, and the oil viscosity is 0.03 Nsec/m^2. The shaft is spinning at 1800 rpm. The Sommerfeld Number as applied in Fig. 11.9 is calculated as:

$$S = \left(\frac{0.03\ \text{N sec}}{\text{m}^2}\right)\left(\frac{(0.1\text{m})(0.05\text{m})}{(222,400\text{N})}\right)\left(\frac{1800\text{rpm}}{60\,\text{sec/ min}}\right)\left(\frac{0.05}{0.00005}\right)^2 = 0.02$$

Note that 'N' as used in the Sommerfeld number calculation is in units of revolutions per minute rather than a surface velocity. From the graph the eccentricity ratio is estimated as 0.89. The shaft offset is thus 0.89 times the radial clearance, or 0.0445 mm. The predicted oil film thickness is thus 0.05 − 0.0445 = 0.0055, or 5.5 micron.

This bearing sizing technique significantly over-predicts the oil film thickness in reciprocating engine bearings (typically by a factor of two or more). Nevertheless, it remains an

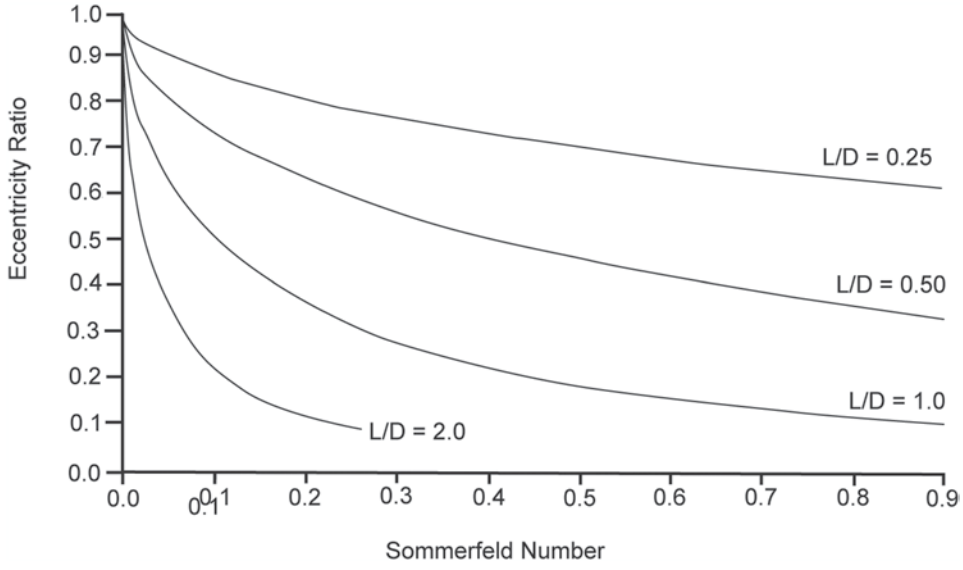

Fig. 11.9 Eccentricity ratio versus Sommerfeld Number as calculated by Reynolds equation for various bearing lengths

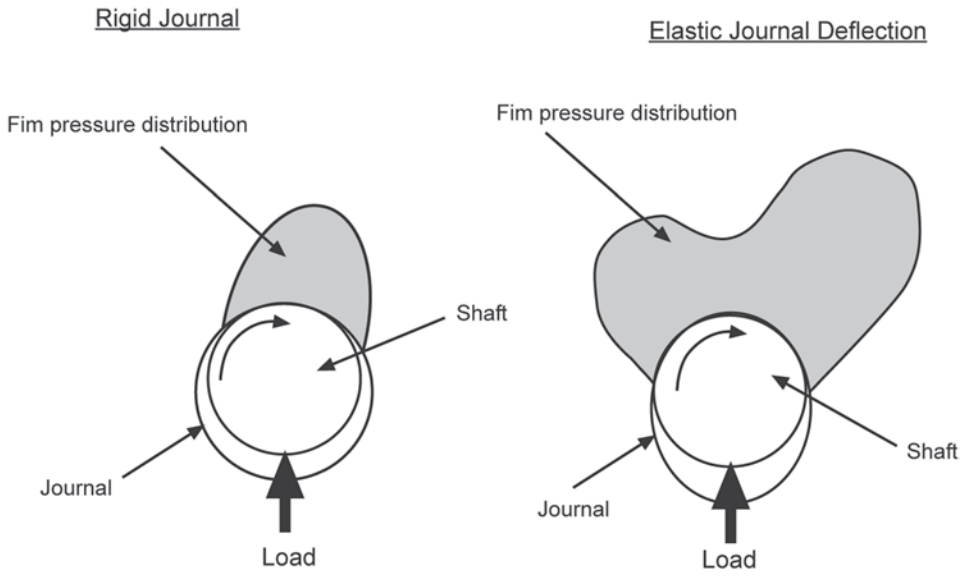

Fig. 11.10 Film pressure distributions for ideal rigid shaft and journal and with significant journal deflection

important tool due to its ease of use, and its effectiveness for relative comparisons. While it may not accurately calculate the actual minimum oil film thickness it can be used to estimate how the film thickness in a new engine will compare to that known to be sufficient in an existing engine.

There are two important reasons for this over-prediction. One is the unsteady loading seen in reciprocating engines. Each rapid load increase forces oil from the bearing, and the dynamic load cycle may not allow the film to fully recover before another rapid load change is experienced. The various deflections of the shaft and journal result in further oil film thickness changes. An important example is shown in Fig. 11.10 where applying a load to a rigid shaft results in journal deflection (exaggerated in the figure). The shaft itself generally deflects much less than the journal. As the shaft is loaded the journal deflects creating pinch points of minimum clearance as shown in the figure. Although the applied load in this case is in the vertical direction two zones of minimum clearance are seen—one in the upstream, and one in the downstream direction. Because the maximum film pressure and minimum film thickness both occur downstream of the direction of loading there is an additive effect on the resulting pressure and film thickness as shown in the figure.

11.5 Dynamic Bearing Sizing

The advent of modern computer capability has allowed automation of the Reynolds solution described in the previous section. Various commercial computer codes are available for predicting oil flow and leakage, film pressure distribution, and oil film thickness

versus both time and position. Most of the available codes are designed to conduct the hydrodynamic calculations, and have options for elasto-hydrodynamic calculations—with significant run-time increases. Several examples of the typical output from such codes are provided in Fig. 11.11 for a connecting rod bearing in an in-line diesel engine. The coordinates chosen for these figures are shown in Fig. 11.11a. The 'x' direction is along

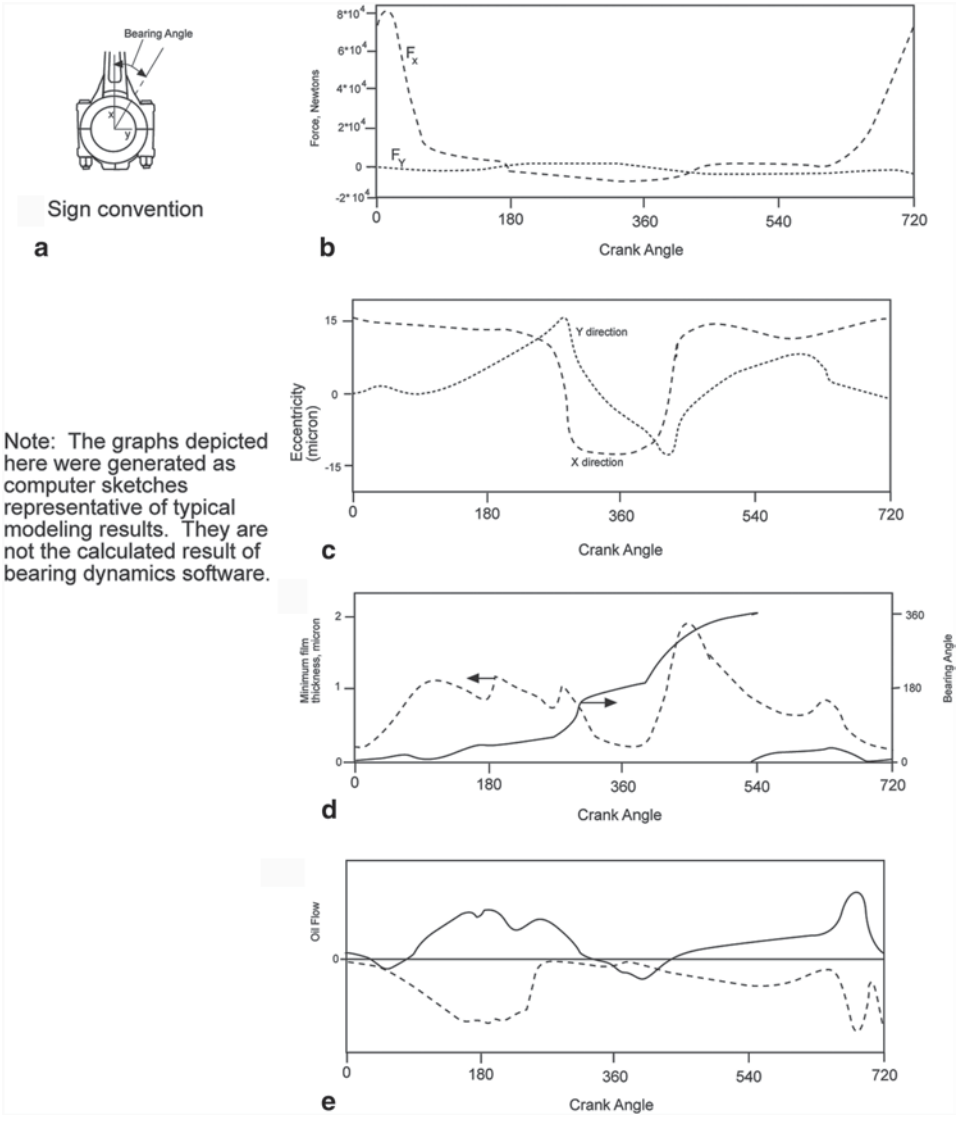

Fig. 11.11 Depiction of example calculations produced with journal bearing design software. Magnitudes and trends representative of diesel engine rod bearing, and rigid journal, hydrodynamic solution

the cylinder axis, and the 'y' direction is through the split between the connecting rod and cap. The 'bearing angle' is chosen relative to the centerline of the rod, with 0° at the center of the rod. Engine crank angle is given relative to TDC between compression and expansion (0°). The applied load is shown in Fig. 11.11b. For this in-line engine it is almost entirely in the 'x' direction, with a slight 'y' direction component in reaction to the piston side forces. This load would be seen to increase with connecting rod length reduction. The next plot (Fig. 11.11c) shows eccentricity in both the 'x' and 'y' directions. Eccentricity is the distance between the shaft and journal centerlines, and is given in microns. The combination of eccentricity in 'x' and 'y' directions results in the minimum oil film thickness, plotted in Fig. 11.11d along with the bearing angle at which it occurs. Notice that one minimum is seen shortly after TDC on the expansion stroke, and that it is located near the center of the bearing shell in the connecting rod. A second minimum occurs 360° crank angle later and is located near the center of the bearing shell located in the rod cap. The final plot (Fig. 11.11e) shows the rates of oil supply to and leakage from the bearing. When carefully validated to experimental results such analysis tools can be used to rapidly assess the effects of design modifications for connecting rod bearings. They can also be used effectively for camshaft bearings.

For the reasons discussed earlier far more effort is needed to couple such tools with block dynamics and crankshaft deflection if one is to predict main bearing performance. An example of such a coupled solution technique is given in Fig. 11.12. Of necessity the complete block model is rather coarse, so accurate predictions at the main bearing journals requires finer sub-models. The coarse and fine models of one bulkhead and main bearing

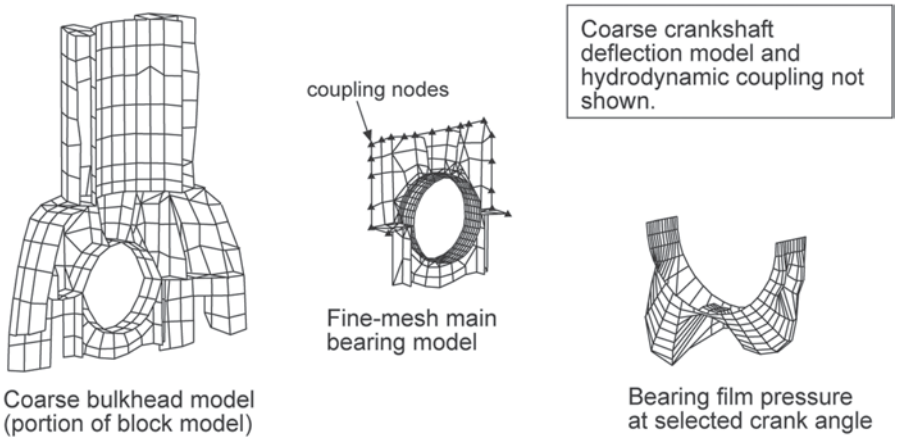

Fig. 11.12 Example of coarse block deflection model, and fine main bearing journal sub-model and resulting film pressure calculation. Based on the models presented by Knoll, G., (see Recommendations for Further Reading)

journal are shown in the figure along with the coupling nodes. Examples of the predicted journal deformation and film pressures are shown in Fig. 11.12c.

Careful engineering judgment must always be applied in bearing computational analysis, recognizing the assumptions that have been made and the effects that may have been ignored. For example, the effect of journal elasticity described previously and often important was ignored in the computations presented in Fig. 11.11. Any misalignment or dimensional variations in crankshaft machining are generally ignored as well. Although bearing analysis tools may provide design guidance engine testing and careful visual assessment remain critical aspects of bearing design validation, and will be further discussed in Sect. 11.7.

11.6 Bearing Material Selection

Ensuring fully hydrodynamic operation involves selecting the combination of contact area and surface finish that will completely separate the bearing from the shaft when the anticipated loads are applied. As power densities increase in many engine applications much attention is now being placed on micro-honing techniques to achieve hydrodynamic operation with thinner oil films. Several other factors must be considered in hydrodynamic bearing design. The factors driving bearing material selection will be discussed in the following paragraphs.

Fatigue Strength Each of the major bearings in a reciprocating engine is exposed to high cycle loads as defined in Chap. 3. Thus the fatigue strength of the bearing material is of crucial importance. The surface of an overloaded bearing will crack with time under fatigue loading. As the cracks spread portions of bearing material will break away, leaving a reduced bearing area and thus further overloading the bearing. Once fatigue cracking initiates the failure mechanism rapidly accelerates due to this material removal.

Scuff Resistance Although the rod, main, and cam bearings are designed to operate under hydrodynamic conditions they experience significant metal-to-metal contact during engine start-up. Under cold conditions, when the oil viscosity may be increased by an order of magnitude or more, the time delay before pressurized oil reaches the bearing may be several seconds. Local friction heating may result in micro-welding and tearing (scuff), or in severe cases seizure and a spun bearing. The bearing has literally welded to the spinning shaft, and the backing tears away from the journal (spins) as the shaft rotates. The propensity of a bearing to bond with the shaft is strongly impacted by material compatibilities, and bearing materials are chosen to minimize bond compatibility.

Wear Rate At the locations where hydrodynamic operation cannot be achieved (piston pins, rocker levers) an overriding material selection criterion is that of low wear rates under high loading with metal-to-metal contact. Wear rate is an important criterion for

hydrodynamic bearings as well. With these bearings the wear occurs only during startup, but the criterion remains important because the engine experiences many cold starts over its lifetime (and in some applications many more hot starts). The primary problem resulting from high wear is loss of oil pressure as the increased clearances allow the oil to flow too quickly from the bearing. The increased clearance also results in impact loading between the shaft and journal, thus accelerating further wear. Some bearing materials have a softer overlay coating, and when the bearing wears they lose this coating.

Conformability Even with careful attention to dimensional tolerances machining variation can result in misalignments that consume the small design clearances required for bearing operation. The bearing material must be much softer than that of the shaft, allowing a new bearing to quickly conform and restore (or approach) design tolerances. This can be done to accommodate small machining variations but does not eliminate the need for careful dimensional control.

Embedability Another problem requiring a soft bearing surface is that of hard particles becoming trapped between the bearing and shaft. It is desired that any dirt and metal particles would be suspended in the lubricant and carried to the filter. However this is not always possible from the confined region of the bearing, and trapped particles can quickly score the bearing and shaft. The problem can be lessened if particles that cannot be removed are instead imbedded in the bearing.

Corrosion Resistance Fuel fragments, sulfur compounds, and oxides of nitrogen are acidic products of combustion, and build up in the oil due to combustion blow-by. Water vapor from combustion and accumulated from the air also build up in the oil. The bearing materials must therefore be resistant to corrosion from both water and acid.

Bearing materials are selected based on the criteria just described, always with the further objective of minimizing cost. Most bearings in use today are referred to as thin-wall bearings, and consist of relatively thin layers of the bearing material bonded to a steel shell. While there are many bearing alloys optimized to meet the most challenging requirements of particular applications they generally fall into three families—white metal bearings alloyed primarily with tin, copper, and antimony; alloys based on aluminum and silicon (often referred to as bi-metal); and the tri-metal bearings consisting of a bronze base and a soft overlay.

The white metal bearings hold the advantages of good scuff resistance and low cost but are limited to low load applications due to their poor fatigue strength. They have good resistance to acid corrosion, but are susceptible to corrosion due to water vapor. Because of the increasing demands placed on new engines this category of bearings is becoming less common.

Bearings alloyed from aluminum and silicon offer good fatigue strength, scuff resistance, and corrosion resistance at reasonable cost. The aluminum-silicon alloy is typically roll plated onto a low carbon steel shell. As silicon content is increased for fatigue

strength the bearing becomes harder and loses conformability and embedability. Historically, aluminum-silicon bearings have not required an overlay, but the frequent stop-start cycles now being applied to many automobile engines make resin overlays attractive. These overlays are further discussed in the following paragraph.

The tri-metal bearing begins with a bronze base, cast or sintered onto the steel shell. The bronze provides excellent fatigue strength, but has high hardness and poor conformability. A soft overlay, until recently almost invariably alloyed from lead, tin, and copper provides scuff resistance and the needed conformability. A thin barrier of nickel is applied between the bronze and the overlay; this is necessary to keep the tin in the overlay from migrating into the bronze and reducing bond strength. There have been several recent advances in overlay materials. Ceramic overlays consisting of aluminum oxide along with copper and lead had become common, but are now being replaced by lead-free aluminum-copper or aluminum-copper-tin alloys, thermally sprayed or sputtered onto the bronze bearing. Another family of coatings is based on molybdenum disulfide resin, sometimes mixed with nylon. These coatings are alloyed with various modifications and applied by physical vapor deposition. The term, ***sputtered bearings,*** is often used among engine designers, and can refer to either the resin or lead-free metal overlays, both of which are applied by sputtering processes. As discussed earlier various resin alloys are now being applied as overlays to aluminum-silicon bearings as well, improving their capability in start-stop applications.

The most common materials for non-hydrodynamic applications are bronze alloys. The contact areas are designed large enough to achieve acceptably low wear rates for the desired engine life. These joints are especially sensitive to oil change interval due to particle build-up in the oil.

11.7 Bearing System Validation

Because of the limitations of analytical approaches discussed earlier experimental validation of each engine bearing system remains a crucial aspect of ensuring the needed durability. Rig testing is attractive due to its simplicity and relatively low cost, and several standard tests have been developed and are widely used. Two examples—the Sapphire test, and the Underwood test are depicted in Fig. 11.13. The Underwood test is especially widely used in the bearing industry. The test mechanically loads the bearing through the use of offset weights on spinning shafts as shown in the figure. The magnitude of the loads can be varied by changing rotational speed and the offset mass. The Sapphire test uses regulated pressure in a piston actuated by the shaft offset. The load magnitude again varies with shaft speed as well as with the regulated pressure. These tests are most effective for bearing material development, and are best used for back-to-back comparisons of a new bearing to an existing bearing. The rig test results do not correlate well to engine tests. One reason for this poor correlation is the difficulty simulating not only the loads but the actual deflections seen in the engine. Another very important reason is that bearing wear

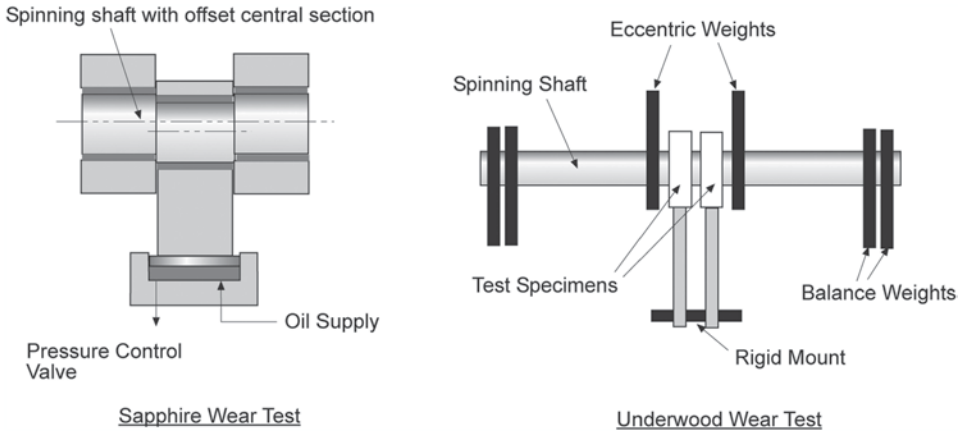

Fig. 11.13 Sapphire and Underwood journal bearing rig tests

is strongly dependent on shaft machining, and especially on whether the shaft is new or is being reused. This is explained by the fact that in a hydrodynamic bearing all of the wear is occurring during start-up, by asperity contact between the shaft and bearing. The surface profile of both parts changes greatly after initial operation. This is an important fact to keep in mind during durability testing conducted in an engine as well. Bearing wear with a newly machined crankshaft will not correlate well to that of replacement bearing shells in the same engine.

In addition to the standard rig tests there are many possibilities for custom tests to address specific design questions. An example test fixture providing various options for piston pin loading is shown in Fig. 11.14. The objectives of any such rig test development must always be carefully thought out. The tests are especially useful in determining the

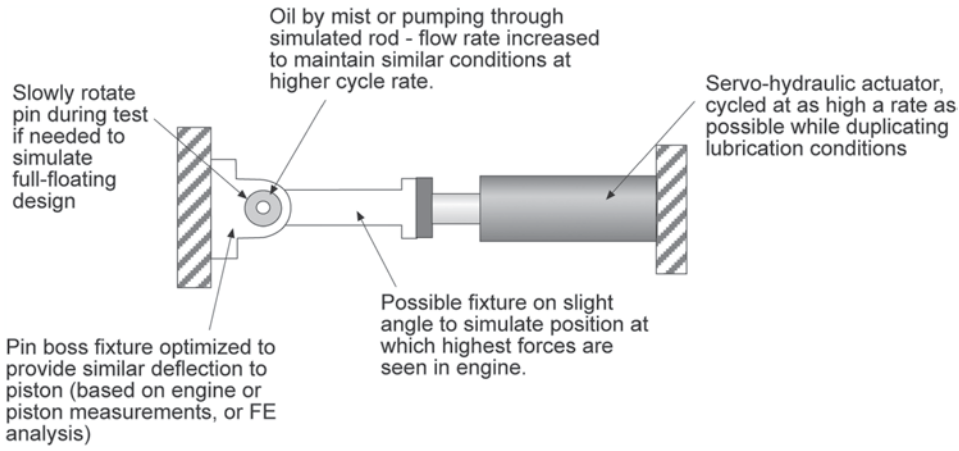

Fig. 11.14 Conceptual layout of a piston pin bushing rig test

limits of a particular bearing or lubricated joint, and in identifying sensitivities to particular variables. Correlation to the actual conditions seen in the engine is far more difficult.

Several categories of engine testing are also important for bearing development. The first is that of further defining the limits of a bearing system. For example, a bearing designed for hydrodynamic operation can be progressively loaded and with careful measurements the maximum load might be identified. In some cases the onset of metal-to-metal contact can be detected through temperature measurement using thermocouples in drillings approaching the running surface from the back of the bearing. A sharper rise in the rate of temperature increase indicates the onset of metal-to-metal contact due to overload.

The second category of engine testing is that of repeated shutdown and restart to generate wear of the hydrodynamic bearing surfaces. The key elements of this cycle are starting the engine and rapidly increasing the load and speed, and then shutting the engine down and allowing the oil to drain back. Various approaches as follows are used to increase the wear rates and reduce total test time:

- Machining back the surface of the bearings to reduce the contact area.
- Externally heating the oil to reduce its viscosity, or cooling it to delay its flow to the bearings.
- Injecting compressed air into the oil rifle to rapidly drain it during each shutdown.

Again, it must be kept in mind that if several tests are to be run with new bearing shells the crankshaft should either be replaced on each test (for most rapid wear), or the same "used" crankshaft should be used for each test.

One might question the purpose of a test designed to generate wear. In the case of tests that repeat the startup and shutdown sequence the typical reason for the test is to ensure that the bearings will not wear out over the startups anticipated over the life of the engine. If the test is accelerated the engineer is then faced with correlating the results from the aggravated test conditions back to "real world" conditions. The best approach for doing this is to compare the results of the new engine or bearing to results obtained under the same aggravated conditions on an existing engine known to perform well in the field.

The third category of engine testing is that done to assess wear rates at non-hydrodynamic bearing locations. Each bearing surface of interest is carefully characterized prior to the test and again at the test's conclusion. Wear rates are maximized by running the tests at high engine speeds and high load (often overloaded) conditions. Wear at these locations is especially sensitive to oil quality, and the wear rates can be further accelerated by running the tests with "dirty" oil, containing carbon and metal particles. Repeatability demands that the particle content of the oil is carefully monitored.

Especially in engine testing visual inspection is an important diagnostic tool and a valuable part of the design validation process. Wear rates, fatigue cracking, corrosion damage, and fretting are all identified through visual inspection. The wear pattern also provides the most direct indication of machining tolerance control problems.

As has been described earlier there are two locations where fretting impacts bearing life. Rod cap separation results in fretting between the rod and cap. This results in loss of running clearance and may ultimately cause bearing scuff or a spun bearing. Movement of the bearing shell in the journal, either because of cap separation or inadequate crush load, results in backside fretting of the bearing shell. This may lead to fatigue cracking of the bearing surface due to loss of support for the bearing shell.

Dimensional control problems can be identified through abnormal bearing wear patterns. Misalignment between the shaft and journal results in concentration of loads along one edge of the bearing. Misalignment between the connecting rod and cap results in loss of clearance and resulting bearing wear at the location of the split in the bearing shells. If the shaft diameter is not maintained constant the bearing wear will be concentrated at the locations of largest shaft diameter. A concave shaft (larger diameter at the edges of the shaft contact region) results in an "hourglass" wear pattern. A convex shaft (larger diameter in the middle of the bearing contact region) results in a "barrel" wear pattern.

Another potential challenge to bearing design is that of cavitation. The general mechanism of cavitation damage was discussed in Chap. 3. It has not been introduced previously in this chapter due to the difficulty of detecting the problem through either measurement or experimentation. It is identified through visual inspection as eroded pinholes. The damage is progressive—as the number and size of the pinholes increases the surrounding material is weakened, resulting in fatigue cracking and material loss. Cavitation damage on lubricated bearings results from a rapid pressure drop followed immediately by a rapid pressure increase. This sequence makes connecting rod bearings most susceptible. Adjusting the bearing clearance slightly can significantly impact cavitation. Oil flow rate and the oil drilling breakout location also have an impact. Bearing computational analysis can sometimes be used to predict the propensity for cavitation damage and to assess the impact of design changes by predicting the rate of film pressure change.

11.8 Recommendations for Further Reading

The references must begin with the classic paper in which the Reynolds formulation for short plain bearings was originally presented (see Ocvirk 1952).

The following text, written in German, provides a detailed look at bearing and lubrication system design (see Affenzeller and Gläser 1996).

There are now many published papers on EHD bearing operation—analytical and experimental. The following are recommended examples for readers interested in further study (see Peixoto and Zottin 2004; Mian and Parker 2004; Sato et al. 2002; Hanahashi et al. 2001; Thomas and Maassen 2001; Okamoto et al. 1999; Ozasa et al. 1995; Priebsch et al. 1995; Torii et al. 1992):

Backside bearing temperature measurements can be an important tool in bearing design. The following paper provides an example of its use (see Suzuki et al. 1995).

Another important question is where to place the oil supply drilling. The following paper presents a study on a rig test with fixed loading. While this is quite different than the situation in a rod bearing (where the oil is supplied through the spinning shaft) it presents the theory (it is also close to the situations of main bearings and cam bearings—they aren't statically loaded, but the oil supply drilling doesn't move). The next paper addresses optimization of the breakout location in crankshaft cross-drillings (see Okamoto et al. 1995; Goenka and Stumbo 1986).

When addressing main bearing analysis one must consider both elasticity of the crankshaft and journal as well as motion of the block bulkheads themselves. The following studies present such computationally intensive coupled solutions (see Knoll et al. 1997; Ebrat et al. 2003).

For a comparative look at plain and roller bearings the following paper addresses their application at the camshaft (see Mackay 2012):

Recent bearing material advances have focused to a great extent on removing lead from the overlays, and simultaneously improving unit load capability (see Nirasawa et al. 2009; Aufischer 2010):

References

Affenzeller, J., Gläser, H.: Lagerung und Schmierung von Verbrennungsmotoren. Springer-Verlag, Wien (1996)

Aufischer, R.: Diesel Engine Bearings for a Lead-Free Future. SAE 2010-32-0060 (2010)

Ebrat, O., Mourelatos, Z., Hu, K., Vlahopoulos, N., Vaidyanathan, K.: Structural Vibration of an Engine Block and a Rotating Crankshaft Coupled Through Elastohydrodynamic Bearings. SAE 2003-01-1724 (2003)

Goenka, P.K., Stumbo, R.F.: A Method for Determining Optimum Crankshaft Oil-Hole Location. SAE 860357 (1986)

Hanahashi, M., Katagiri, T., Okamoto, Y.: Theoretical Analysis of Engine Bearing Considering Both Elastic Deformation and Oil Film Temperature Distribution. SAE 2001-01-1076 (2001)

Knoll, G., Schönen, R., Wilhelm, K.: Full Dynamic Analysis of Crankshaft and Engine Block with Special Respect to Elastohydrodynamic Bearing Coupling. ASME 97-ICE-23 (1997)

Mackay, S.: Comparison Between Journal and Rolling Element Bearings in a Camshaft Application. SAE 2012-01-1324 (2012)

Mian, O., Parker, D.: Influence of Design Parameters on the Lubrication of a High Speed Connecting Rod Bearing. SAE 2004-01-1599 (2004)

Nirasawa, T., Yasui, M., Ishigo, O., Kagohara, Y., Fujita, M.: A Study of Lead-free Al-Zn-Si Alloy Bearing with Overlay for Recent Automotive Engines. SAE 2009-01-1054 (2009)

Ocvirk, F.W.: Short-Bearing Approximation for Full Journal Bearings. NACA Technical Note 2808 (1952)

Okamoto, Y., Mochizuki, M., Mizuno, Y., Tanaka, T.: Experimental Study for the Oil Flow Supplied from Oil Hole on Statically Loaded Bearings. SAE 950947 (1995)

Okamoto, Y., Kitahara, K., Ushijima, K., Aoyama, S., Xu, H., Jones, G.: A Study for Wear and Fatigue of Engine Bearings on Rig Test by Using Elastohydrodynamic Lubrication Analysis. SAE 1999-01-0287 (1999)

Ozasa, T., Yamamoto, M., Suzuki, S., Nozawa, Y., Kononi, T.: Elastohydrodynamic Lubrication Model of Connecting Rod Big End Bearings; Comparison with Experiments by Diesel Engine. SAE 952549 (1995)

Peixoto, V.J.M., Zottin, W.: Numerical Simulation of the Profile Influence on the Conrod Bearings Performance. SAE 2004-01-0600 (2004)

Priebsch, H., Loibnegger, B., Tzivanopoulos, G.: Application of an Elastohydrodynamic Calculation Method for the Analysis of Crank Train Bearings. ASME 94-ICE-1 (1995)

Sato, K., Makino, K., Machida, K.: A Study of Oil Film Pressure Distribution on Connecting Rod Big Ends. SAE 2002-01-0296 (2002)

Suzuki, S., Ozasa, T., Yamamoto, M., Nozawa, Y., Noda, T., O-hori, M.: Temperature Distribution and Lubrication Characteristics of Connecting Rod Big End Bearings. SAE 952550 (1995)

Thomas, S., Maassen, F.: A New Transient Elastohydrodynamic (EHD) Bearing Model Linkable to ADAMS®. SAE 2001-01-1075 (2001)

Torii, H., Nakakubo, T., Nakada, M.: Elastohydrodynamic Lubrication of a Connecting Rod Journal Bearing in Consideration of Shapes of the Bearing. SAE 920485 (1992)